Concentration Regimes for Extensional Relaxation Times of Unentangled Polymer Solutions

Diego D. Soetrisno,[†] Carina D. V. Martínez Narváez,[‡] Vivek Sharma,^{*,‡} and

Jacinta C. Conrad^{*,†}

 $\dagger Department$ of Chemical and Biomolecular Engineering, University of Houston, Houston, TX

‡Department of Chemical Engineering, University of Illinois Chicago, Chicago, IL

E-mail: viveks@uic.edu; jcconrad@uh.edu

Abstract

We study the extensional flow properties of polyacrylamide (PAM) solutions with various molecular weights and dispersities using a dripping-onto-substrate (DoS) protocol. A recent study [Dinic and Sharma, Macromolecules 2020, 53, 4821 – 4835] suggested that coil-stretch hysteresis, which occurs when the drag coefficient ratio of stretched and coiled polymer chains $\varsigma_s/\varsigma_c > 4.5$, controls the scaling exponent of the extensional relaxation time λ_E with concentration. Here, we test this hypothesis by varying ς_s/ς_c through the PAM molecular weight distribution. The scaling exponent of the concentration dependence of λ_E is m = 0.34 for PAM solutions with $\varsigma_s/\varsigma_c < 4.5$ and m > 0.5 for PAM solutions with $\varsigma_s/\varsigma_c > 4.5$. The increase in scaling exponent is attributed to the presence of coil-stretch hysteresis, which screens the excluded volume

interactions under extensional flow. For highly disperse solutions with $\mathfrak{D} \approx 21$, the transition from an exponent of 0.67 to 1 occurs at overlap concentration c^* derived from the weight-averaged molecular weight instead of viscosity-averaged molecular weight, highlighting the role of long chains. These results provide insight into the role of the polymer size distribution for the concentration-dependent extensional material response in dilute and unentangled semidilute solutions.

Introduction

Understanding the role of polymer concentration on the rheology of polymer solutions ¹⁻⁶ is of great interest for applications such as electrospinning ⁷ and 3-D printing. ⁸ The concentration-dependent variation in the static and dynamic properties of macromolecules in solution depends on polymer-solvent interactions, polymer flexibility, and polymer molecular weight. ^{2,5,9} Under quiescent conditions, the volume available per coil in a polymer solution equals the unperturbed coil size at the so-called overlap concentration c^* . The different concentration regimes are determined by whether the polymer coils overlap with each other in the solution, ^{1,2} and are typically divided into dilute ($c < c^*$), unentangled semidilute ($c^* < c < c_e$), and entangled ($c > c_e$) regimes, ¹ where c_e is the entanglement concentration. ^{2,5}

In the dilute regime $(c < c^*)$, the polymer coils do not overlap and the shear rheology is primarily determined by intrachain hydrodynamic interactions (HI) and excluded volume (EV) interactions. Both forces are modulated by polymer-solvent interactions as captured by Zimm theory³ and not by interactions between the coils. Both HI and EV interactions are progressively screened in the semidilute regime $(c > c^*)$, where blob models are used to describe the chain dynamics and shear rheology response. The effect of local interactions is included via the Zimm model for dynamics within a blob, whereas the global dynamics of an idealized chain of blobs are described using Rouse dynamics. The number and size of blobs are determined self-consistently for equilibrium, overlapping coils using scaling theory.

In entangled solutions ($c > c_e$), the topological constraints or entanglements give rise to extremely slow chain dynamics. The diffusion coefficient D, zero-shear viscosity η_0 , and shear relaxation time λ_s show distinct transitions at c^* and c_e as a function of concentration. Though the shear rheology response of unentangled polymer solutions exhibits universal characteristics, 2,5,9 the corresponding macromolecular parameters and shear rheological measures fail to capture the variation and range of effects that are present in processing. 10,11 These involve materials performances commonly associated with jettability, sprayability, mist formation during coating, stringiness, and spinnability.

Processing operations and applications such as drop formation during jetting or spraying, fiber spinning, coating, and flow through porous media involve streamwise velocity gradients associated with extensional flows. ^{10–13} Macromolecules can undergo significantly higher degrees of stretching and orientation in response to extensional flow, influencing their chain dynamics, the degree of overlap, and extensional relaxation time λ_E . ¹⁴ Unentangled solutions of flexible polymers often display strain hardening, and extensional viscosity η_E values can be several orders of magnitude higher than shear viscosity $\eta(\dot{\gamma})$, even though for Newtonian fluids $\eta_E = 3\eta$.

Polymer coils are only mildly perturbed in response to shear flow. It is well-established, however, that polymers can undergo significant stretching in response to extensional flow, leading to a coil-stretch transition beyond a critical extension rate $\dot{\varepsilon}_{C\to S}$. Earlier studies in the 1970s postulated that the coil-stretch transition occurs in macromolecules if the ratio of deformation rate to the relaxation rate (of unperturbed coils, λ_s) exceeds 1/2. Furthermore, theoreticians predicted the existence of coil-stretch hysteresis such that the pre-stretched chains relax back or undergo the stretch-coil transition $\dot{\varepsilon}_{S\to C} < \dot{\varepsilon}_{C\to S}$ (at a lower deformation rate). Works done decades after provided evidence for both the coil-stretch transition and hysteresis by visualizing conformation changes in fluorescently labeled DNA using precision microfluidics experiments. ^{18,19} Thereafter, several studies carried out

simulations to determine that coil-stretch hysteresis manifests if the ratio of drag coefficients of the stretched to unperturbed coils exceeds a critical value of $\zeta_s/\zeta_c > 4.5$. ^{18–22} Polymer chains exhibit entropic resistance to stretching and conformation-dependent drag depend nonlinearly on the degree of stretching, deformation history, and initial conditions. Coil-stretch hysteresis arises as large polymer molecules can be kinetically trapped in either coil or extended state. The hysteresis disappears at high enough polymer concentrations where hydrodynamic interactions are fully screened, and the frictional drag coefficient is thus independent of polymer conformation. ²³ More recently, Ref. 24 postulated that the coil-stretch transition and hysteresis can influence the time-dependent decrease in the radius of liquid necks undergoing capillary-driven pinching and the concentration-dependent variation of λ_E .

When the polymer chain conformation changes from coiled to stretched, HI are progressively screened ¹⁵ and the previous simple physical picture describing the magnitude and concentration regimes of λ_E may no longer hold. Indeed, in stretched configurations polymer chains overlap at concentrations $c \ll c^*$. ²⁵ Under strong extensional flow, a stretched single chain behaves like a Rouse chain of tension blobs and retains HI and EV interactions captured by the Zimm model below the length scale of a tension or Pincus blob. ²⁶ In the single chain limit, the size of a tension blob depends on the stretching force. The overall drag depends on conformation and change in HI. Thus, after strong extensional flow stretches polymer chains, interchain interactions manifest even for the nominally dilute regime defined via c^* determined using unperturbed coil size. ^{27,28} The dilute terminology is thus valid only below the stretched overlap concentration c_s^* , where individual chains can fully deform without interacting with other chains. ^{24,25,29}

Only thermodynamic considerations determine blob size for the "intrinsically" semidilute solutions ($c > c^*$), so defined by Ref. 30, to emphasize overlap of unperturbed coil. As blob size and number are governed by degree of stretching, however, interchain interactions in the response to extensional flows as well as λ_E are sensitive to macromolecular strain

and extensibility L_E . Extensibility is defined as $L_E = L_c/R_{us}$, the ratio of full stretched or contour length L_c to unperturbed chain size or unstretched length R_{us} , or as $L_E = N_k^{(1-\nu)}$, a function of the number of Kuhn segments N_k and the Flory exponent ν .

Progress in connecting macromolecular properties to rheological and processing behavior was hampered by longstanding challenges in characterizing the extensional rheology response and the lack of both experimental data and theoretical results on stretched chain hydrodynamics (beyond the single chain limit). Refs. 24,30–33 introduced dripping-onto-substrate (DoS) rheometry protocol as a technique that provides a frugal measurement of elasticity (or λ_E) and η_E . Under extensional flow, polymer chains relax exponentially from elongational stress on a characteristic timescale, λ_E , ^{13,34} that can be observed experimentally only at concentrations above a minimum concentration c_{\min} required to measure the elastic contribution of the polymer.³⁵ In the dilute regime defined via c^* , $\lambda_{\rm E}$ exhibits a power-law dependence $\lambda_{\rm E} \propto c^m$ that deviates from the predicted linear concentration dependence for the Rouse mode of relaxation in dilute solutions $\lambda = \lambda_{RZ}(1 + k_H[\eta]c)$, where λ_{RZ} is the infinite dilution lifetime and k_H is the Huggins constant, 30,36 due to chain interactions. Refs. 24,30 postulated that the dynamics of semidilute polymer solutions described by a Rouse-Zimm chain model could be employed to rationalize the scaling relations of dilute stretched chains in extensional flow. In blob theory, 1,5,37 the concentration dependence of the relaxation time of a Rouse-Zimm chain scales as 30

$$\lambda \approx \frac{\eta_s b^3}{kT} \left(\frac{N_k b_k^3 N_A}{M_w} \right)^m c^m, \tag{1}$$

where $m = (2-3\nu)/(3\nu-1)$. Under this framework, Refs. 24,30 related the limiting values of m determined from eqn. 1 to the EV interactions: the value of 0.31 for a good solvent (for which the Flory exponent $\nu = 0.588$) implies the presence of EV interactions, whereas the value of 1 for a theta solvent ($\nu = 1/2$) implies full screening of EV interactions due to chain stretching.

Most power-law exponents measured in extensional flow experiments, however, fall between the two limits, 35,38 suggesting that quantitative prediction requires understanding of the additional effects that are present due to elongational flow but not considered in blob theory. Previous studies on polyethylene oxide (PEO) in water 31 and glycerol-water mixtures 38 (good solvents) observed a power-law exponent of m = 0.65. A study on polystyrene 35 found an exponent of m = 0.58 in diethylphthalate (near good solvent) and m = 0.89 in styrene monomer (near theta solvent). Studies on polyacrylamide 39 and partially hydrolyzed polyacrylamide 40 solutions in water, glycerol, and their mixtures found exponents m = 0.77 - 0.89.

Towards this end, Refs. 24,30 connected the concentration dependence of the extensional relaxation time $\lambda_{\rm E}$ for $c < c^*$ to polymer macromolecular properties. ²⁴ The elastic responses of polyethylene oxide (PEO) and 2-hydroxyethyl cellulose (HEC) solutions were measured as a function of concentration and compared to predictions in concentration regimes delineated by c_{\min} and a stretched overlap concentration c_s^* . The parameter c_s^* was derived from the theory for rod-like polymers in the semidilute regime² based on macromolecular parameters. Although both polymers have the same c^* , PEO is more flexible and extensible than HEC based on their estimated contour length L_c , Kuhn length b_k , and unperturbed coil length $R_{
m us}$ values. For HEC, $m_{
m HEC} = 0.32$ at $c^* < c < c_{
m e}$ is close to the prediction from blob theory. For PEO, however, $m_{\rm PEO} = 0.65$ at $c_s^* < c < c^*$ is the geometric mean of the two limits of the blob theory prediction. The values of the exponents suggested that EV interactions govern the extensional response in HEC, whereas chain stretching partially screens the EV interactions in PEO. The differences in exponent were attributed to the extent of screening of EV interactions due to coil-stretch hysteresis of the polymer chains. 24,30 Coilstretch hysteresis occurs when the ratio of the drag coefficients of stretched ς_s and coiled ς_c chains exceeds $\zeta_s/\zeta_c > 4.5$. ^{15,18,20} It is incompletely understood, however, how controlling the polymer size distribution may alter the concentration-dependent response by modifying the extent of coil-stretch hysteresis.

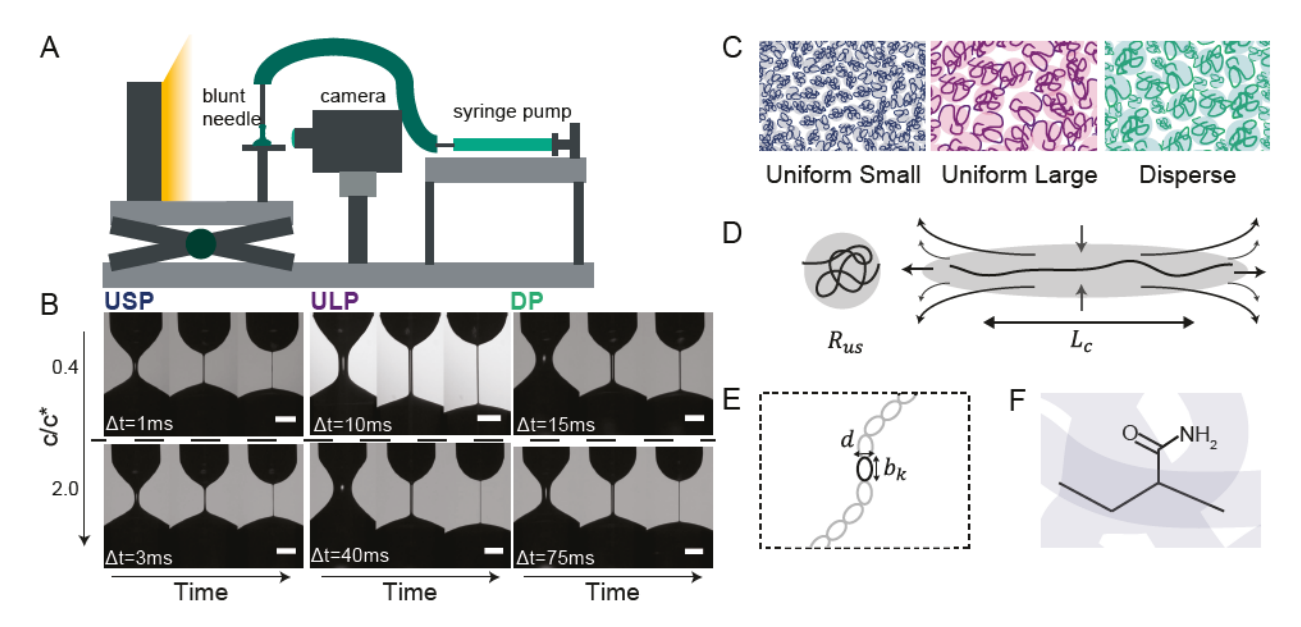


Figure 1: Pinching dynamics of PAM solutions investigated using a Dripping-onto-Substrate (DoS) protocol. (A) Schematic of DoS setup used in this study includes high-speed imaging of a polymer solution liquid bridge over time undergoing a capillary-driven instability. (B) Images of pinch-off dynamics of PAM solutions reveal that the breakup time for DP solutions is greater than that for USP and ULP solutions at equal c/c^* . Scale bars are 0.5 mm. (C) Diagrams of varying polymer molecular weight and polydispersity investigated in this study: uniform small polymer (USP), uniform large polymer (ULP), and disperse polymer (DP). (D) Length scales of polymer in quiescent coiled state (unstretched length $R_{\rm us}$) and stretched state (contour length $L_{\rm c}$) (E) Macromolecular properties of polymer defined from their Kuhn segments: Kuhn length $b_{\rm k}$ and diameter d (F) Chemical structure of the monomer building block of PAM.

Practical applications also require understanding the role of the molecular weight distribution on the extensional flow properties. The extensional rheology response is particularly sensitive to L_E , and often highly extensible chains are added to formulations to improve stringiness and spinnability. All Recent studies found that the spinnability parameter of disperse polymer solutions are better predicted from an extensibility-averaged molecular weight $M_{\rm L}$ than weight-averaged $M_{\rm w}$ or number-averaged molecular weight $M_{\rm n}$. All How the concentration regimes of stretched polymer chains change with dispersity and whether the prediction from macromolecular parameters is sufficient remain open questions. Fundamental understanding of the different concentration regimes of extensional relaxation time and their dependence on the polymer molecular weight distribution will enable better control over the processability

of materials. 45

In this contribution, we use a modified DoS rheometry protocol (Fig. 1A-B) based on Refs. 24,30–33 to measure λ_E of unentangled polyacrylamide (PAM) solutions, and we elucidate the influence of molecular weight and dispersity on concentration-dependent variation in λ_E . Polyacrylamide is a linear water-soluble polymer often used in turbulent drag reduction, ⁴⁶ as a viscosifier for enhanced oil recovery, ⁴⁷ and for biocompatible fiber materials. ^{48,49} We find that concentration regimes of extensional relaxation time λ_E for PAM depend on the polymer physical properties derived from intrinsic viscosity measurements and molecular weight. The extensional response of PAM solutions was better predicted with $M_{\rm w}$, especially for a highly disperse solution, highlighting the importance of long polymer chains. The extensional behavior is consistent with other polymer systems (PEO and HEC), ²⁴ implying that concentration-dependent response can be controlled through polymer size and dispersity.

Materials and Methods

We prepared three series of solutions of PAM with various molecular weight and dispersity: $M_w = 194$ kDa, D = 1.24, Polymer Source, Uniform Small Polymer (USP); $M_w = 1.00$ MDa, D = 1.25, Polymer Source, Uniform Large Polymer (ULP); and $M_w = 1.97$ MDa, D = 21, Sigma-Aldrich, Disperse Polymer (DP) (Fig. 1C). The differences in polymer size will consequently lead to variation in the unstretched length or coil length R_{us} and stretched length or contour length L_c of the polymer (Fig. 1D). Additional length scales, such as the Kuhn length b_k and diameter d (Fig. 1E) as well as the monomer length l_0 , bond length l, and monomer molecular weight M_0 (Fig. 1F), are assumed to be constant across the three PAM. Polymer powder was dissolved into 80 w/w% glycerol-water to make stock solutions, which were mixed at low speed (~ 7 rpm) on a roller to prevent chain scission $^{50-52}$ for at least one week to ensure homogenization.

The shear viscosity η as a function of shear rate $\dot{\gamma}$ was measured with a DHR-2 Rheometer (TA Instruments, New Castle, DE) with minimum torque $2\mu N \cdot m$ on a 40 mm diameter cone-and-plate hard-anodized aluminum geometry. Polymer solutions were treated with a consistent preshear protocol⁵³ before every flow sweep (SI). We used a DoS protocol (Fig. 1A-B) modified from that in Refs. 31,32 (SI) to characterize the extensional rheology response due to the low viscosity and low elasticity of most of our PAM solutions.

Results and Discussion

The steady shear viscosity of the three solutions (USP, ULP, and DP) is nearly independent of shear rate in the dilute regime $(c/c^* = 0.4, \text{ estimated from } c^* \approx 1/[\eta])$ (Fig. 2A). ULP and DP solutions exhibit shear-thinning behavior in the semidilute regime $(c/c^* = 2.0)$, whereas the USP solution exhibits a Newtonian-like response. The specific viscosity $\eta_{sp} = (\eta_0 - \eta_s)/\eta_s$, where η_0 is the viscosity measured at the lowest accessible shear rate and η_s is the solvent viscosity, collapses onto a master curve as a function of normalized concentration c/c^* (Fig. 2B). The linear concentration dependence in the dilute regime $\eta_{sp} \sim (c/c^*)^1$ and quadratic scaling of $\eta_{sp} \sim (c/c^*)^2$ in the semidilute unentangled regime are consistent with scaling theory predictions for neutral polymers. ⁵ The scaling behavior and master curve are similar to those obtained in an earlier study of aqueous PAM solutions. ⁵⁴

The physical properties of PAM solutions were calculated from molecular weight and the intrinsic viscosity $[\eta]$ (SI). The excluded volume exponent for PAM in 80 w/w% glycerol-water, estimated from $[\eta]$ via the Mark-Houwink equation (SI), is $\nu \sim 0.6$, suggesting that 80 w/w% glycerol-water is a good solvent for PAM. The viscosity-averaged molecular weight M_v of DP calculated from $[\eta]$ is 570 kDa, consistent considering the large dispersity of the sample.

Using a modified DoS protocol (Fig. 1A and SI), we determined the time-dependent evolution

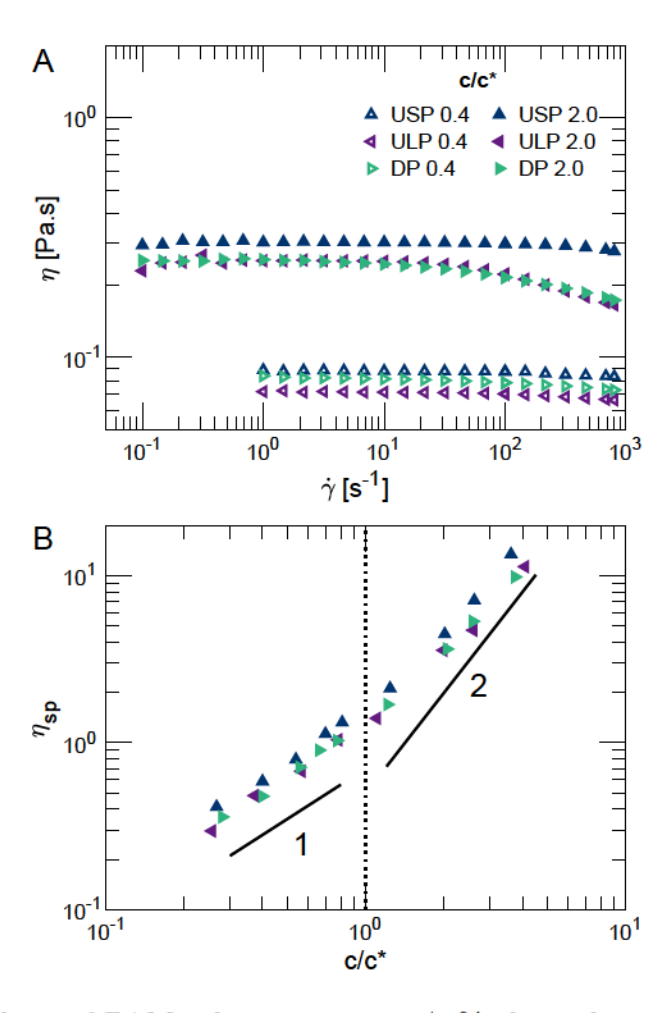


Figure 2: Shear rheology of PAM solutions in 80 w/w% glycerol-water with 1.5 mM NaCl. (A) Flow curves of representative USP, ULP, and DP polyacrylamide solutions at matched c/c^* in the dilute and semidilute unentangled regimes. (B) Specific viscosity $\eta_{\rm sp}$ of PAM solutions as a function of normalized concentration c/c^* . Data from all three solutions collapsed onto a master curve, as expected for neutral polymer rheology.

of the neck radius for the polymer solutions. Images of the filament breakup for USP, ULP, and DP solutions of equal c/c^* reveal that the DP solution exhibits the longest breakup time (Fig. 1B). We extracted the time-dependent filament radius from the images. High-viscosity Newtonian fluids such as the background solvent exhibit a viscocapillary (VC) response, 13,55,56 for which

$$\frac{R(t)}{R_0} = \frac{(2X_{\rm vc} - 1)}{6} \left(\frac{\sigma}{\eta_0 R_0}\right) (t_f - t) \tag{2}$$

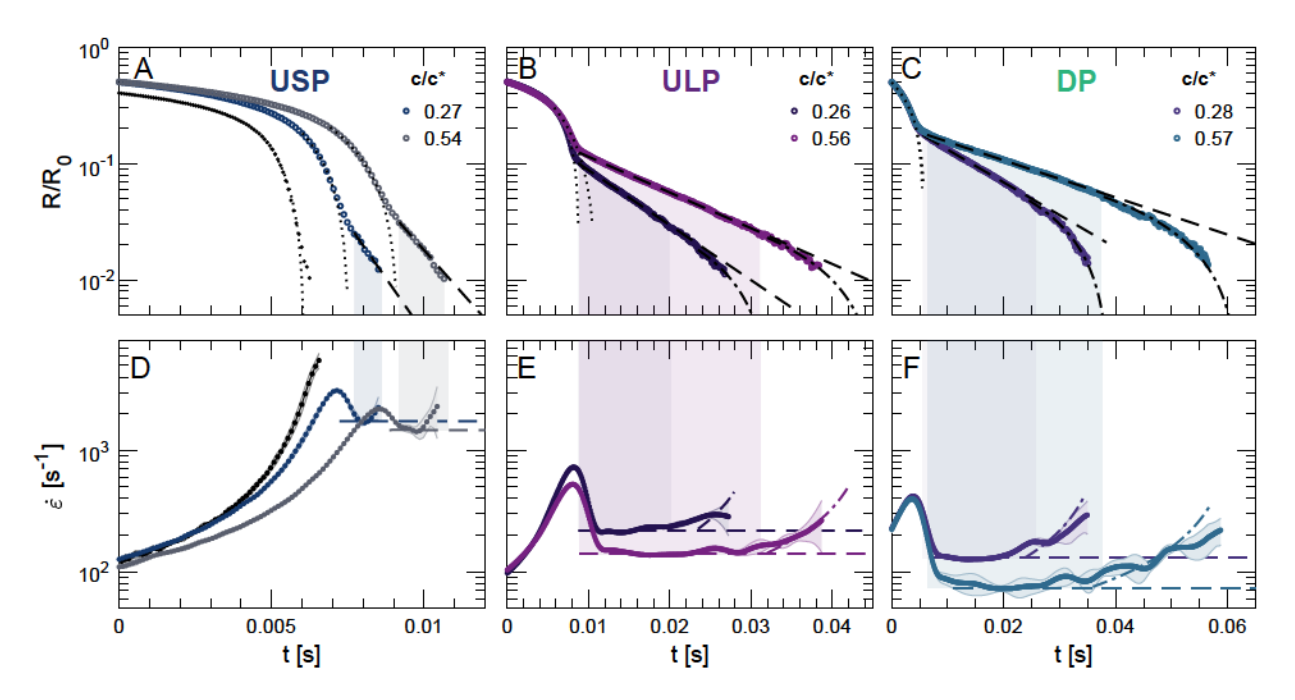


Figure 3: Radius evolution of (A) USP, (B) ULP, and (C) DP polyacrylamide solutions in 80 w/w% glycerol-water as a function of time. Dotted lines in (A) indicate viscocapillary (VC) scaling and in (B) and (C) indicate power-law (PL) scaling. Dashed lines indicate elastocapillary (EC) scaling and the shaded area indicates the EC regime. Dash-dotted lines indicate terminal viscoelastocapillary (TVEC) scaling. The derivative of the radius evolution $\dot{\varepsilon} = (-2/R)(dR/dt)$ for (D) USP exhibits a peak followed by a plateau or slight decrease; for (E) ULP and (F) DP, $\dot{\varepsilon}$ exhibits a sharp decrease and a constant strain rate upon reaching the EC regime and a subsequent increase upon entering the TVEC regime prior to pinch-off. Errors in strain rate are derived from averaging multiple replicates at matched peak $\dot{\varepsilon}$. For polymer solutions we define t=0 as the time at which $R/R_0=0.50$; for the solvent (black circle) we define t=0 as the time at which $R/R_0=0.40$.

where σ is the surface tension, η_0 is the zero-shear viscosity, R_0 is the nozzle radius, X_{vc} is a numerical prefactor⁵⁷ that varies across experiments and is of $\mathcal{O}(1)$, ⁵⁸ and t_f is the total filament timespan.

The dominance of viscous forces during pinch-off is typically predicted from the Ohnesorge number $Oh = \eta_0/(\rho\sigma R_0)^{1/2}$, which compares the magnitude of the viscous forces to those of the inertial and surface tension forces. When Oh > 1, the time evolution of the radius follows VC scaling. By contrast, Newtonian fluids with Oh < 1 instead exhibit an inertio-capillary

(IC) $response^{56,59,60}$ for which

$$\frac{R(t)}{R_0} = X_{ic} \left(\frac{\sigma}{\rho R_0^3}\right) (t_f - t)^{2/3}$$
 (3)

where ρ is fluid density and $X_{\rm ic}$ is a $\mathcal{O}(1)$ numerical prefactor with various experimentally determined values. ⁵⁸ Both VC and IC equations are adapted from Ref. 56.

We use a generalized power-law (PL) relationship^{30,56} to estimate the scaling exponent of our samples without prior assumption on their scaling response, given as

$$\frac{R(t)}{R_0} = Y(t_f - t)^{n_e} \tag{4}$$

where n_e is the power-law exponent and Y is a constant that represents the material intrinsic properties. From this fitting,p we observe VC scaling at the later part of the pinch-off process for our glycerol-water solvent (Fig.3A) despite having Oh = 0.17, because the filament radius approaches the Ohnesorge unit length $l_{\rm Oh} = \eta^2/(\sigma\rho) = 38~\mu{\rm m}.^{58}$

By contrast, the pinching dynamics of PAM solutions display an initial regime that scales with a power-law (PL) exponent followed by a second regime that exhibits an elastocapillary (EC) response, in which the filament radius decays exponentially with time according to ^{13,61}

$$\frac{R(t)}{R_0} = \left(\frac{G_E R_0}{2\sigma}\right)^{1/3} \exp[-(t - t_c)/3\lambda_E] \tag{5}$$

where G_E is the elastic modulus and t_c is the transition time from PL to EC response. The prefactor corresponds to the critical radius $R_c \approx R_0 (G_E R_0/2\sigma)^{1/3}$ of the transition. The distinct radius evolution profile of PL and EC response for PAM solution is illustrated in Fig. 3A-C, where the radius evolution transitions from a linear to an exponential scaling for all PAM solutions.

At $t = t_c$, ULP and DP (Fig. 3B and C) exhibits a much sharper transition to the EC than

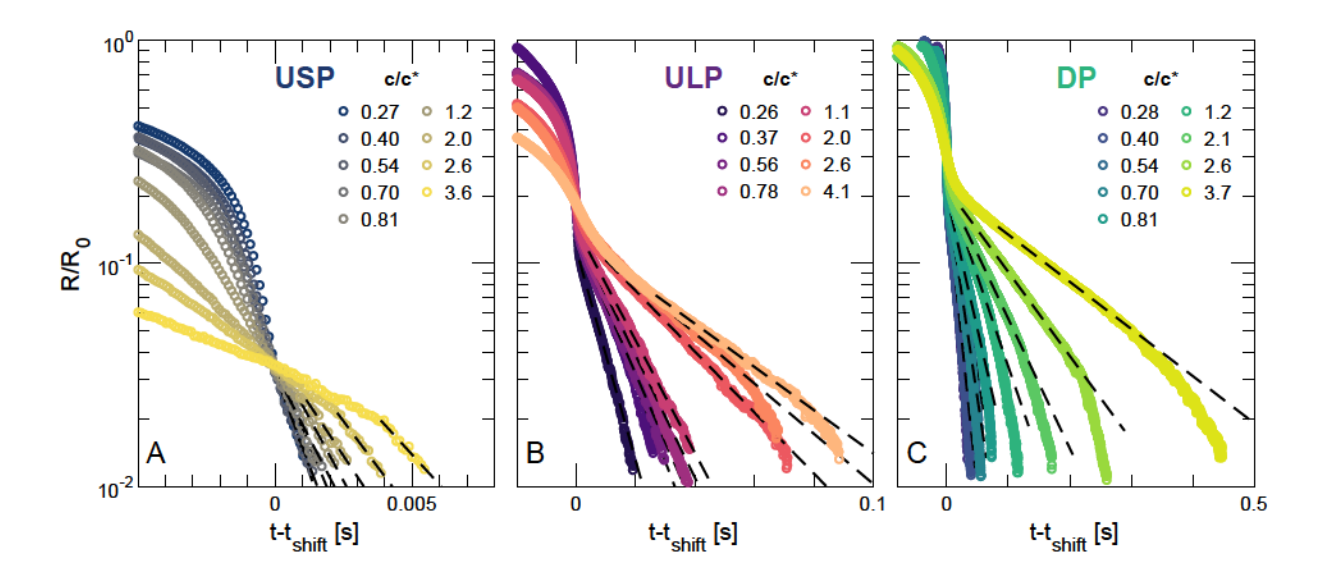


Figure 4: Pinching dynamics of USP, ULP, and DP polyacrylamide solutions in 80 w/w% glycerol-water with 1.5 mM NaCl. Neck radius evolution shifted by $t_{\rm shift}$ displays a concentration-dependent EC response. We define $t_{\rm shift}$ as the time at which $R/R_0 = 0.03$ for USP, $R/R_0 = 0.18$ for ULP, and $R/R_0 = 0.30$ for DP. Dashed lines indicate EC fitting (eqn. 5).

does USP (Fig.3A). The magnitude of change in radius evolution scaling is quantified from the derivative of R/R_0 with time, from which extensional strain rate $\dot{\varepsilon} = (-2/R)(dR/dt)$ is determined. The strain rate magnitude of USP attains a peak at the transition to the EC regime and subsequently plateaus or slightly decreases as pinch-off is reached (Fig. 3D). By contrast, $\dot{\varepsilon}$ for ULP and DP also exhibit similar peaks but thereafter decrease abruptly to a constant value throughout the EC regime (Fig. 3E,F.). Ref. 24 suggests that this sharp decrease is a signature of the coil-stretch transition. We also observe another qualitative discrepancy on long timescales, where the terminal visco-elastocapillary (TVEC) regime ^{13,33} is absent in USP but prominent in ULP and DP. On long timescales, the scaling regime deviates from exponential and is instead linear $(R/R_0 \sim (t_f - t))$ due to finite extensibility effect. The slope from the TVEC scaling follows $\sigma/2R_0\eta_{E,\infty}$, and we confirmed that the terminal steady-state extensional viscosity $\eta_{E,\infty}$ from the TVEC fitting matches the η_E calculated from the numerical derivation ($\eta_E = -\sigma/2dR/dt$). The differences in EC and TVEC regime time span between ULP and DP may arise from the system polydispersity.

The mixtures of short and long chains in DP potentially allow the bulk solution to experience a finite extensibility effect at an earlier stage compared to a solution of lower dispersity.

To illustrate the concentration-dependent elastic response, we shift the radius evolution with $t_{\rm shift}$. All three PAM solutions exhibit an elastic response that follows the EC scaling (Fig. 4) in the dilute regime for concentrations greater than c_s^* . USP solutions exhibit a weaker EC response (i.e., a weaker exponential decay) than ULP or DP solutions. Very dilute ULP and DP solutions with $c < c_s^*$ exhibit a similar short EC regime and transition close to pinch off. The difference in the qualitative shape of the time evolution of the filament radius for USP versus ULP and DP may arise from the weaker elastic contribution of USP in comparison to the larger polymers.

By fitting the exponential decay with eqn. 5 (dashed lines), we quantify the elastic response via λ_E . To compare the different elasticity measure for dilute solutions, we calculate the Zimm relaxation time $\lambda_z = [\eta] \eta_s M_w / U_{\eta\tau} RT$, where the prefactor $U_{\eta\tau} = \sum_{i=1}^{\infty} \frac{1}{i^{3\nu}}$ is the universal ratio. 6,35 The estimated values of λ_z for USP, ULP and DP are respectively 0.19, 3.8, and 4.8 ms. The λ_E values for USP never fall below the predicted λ_z at very dilute concentrations, whereas λ_E for ULP and DP continue to decrease with concentration and can be up to an order of magnitude smaller than λ_z . These results are consistent with measurements for polystyrene in styrene oligomer 35 and for a similar system of PAM in glycerol-water mixtures. 40 The comparison emphasizes the distinct concentration-dependent timescale that governs polymer relaxation under stretching flow.

Representative parameters for both shear and extensional measurement are tabulated in Table 1, where background solvent of 80 w/w% glycerol-water is measured to have Oh = 0.17. The Ohnesorge number of the solutions transition from $\mathcal{O}(0.1)$ to $\mathcal{O}(1)$ with increasing polymer concentration. This result indicates a transition from inertial- to viscous-dominated dynamics, which may contribute to the differences in the Newtonian regime prior to elastic response in Fig. 4. Polymer size strongly affects R_c , which results in scaling differences

Table 1: Rheological parameters measured for each polymer at similar c/c^* from shear and extensional measurements. Background solvent viscosity η_0 of 80w/w% glycerol-water is measured at 0.056 Pa·s.

\boldsymbol{c}	η_0	Oh	R_c	$oldsymbol{t_c}$	t_f	λ_E			
(g/L)	$(Pa \cdot s)$		$(\mu \mathrm{m})$	(ms)	(ms)	(ms)			
USP									
3.2	0.079	0.25	45 ± 5	7.5 ± 0.1	8.5 ± 0.06	0.39 ± 0.004			
6.5	0.10	0.31	56 ± 4	8.3 ± 0.5	9.7 ± 0.6	0.46 ± 0.03			
9.9	0.13	0.40	49 ± 7	9.3 ± 0.3	11 ± 0.2	0.53 ± 0.05			
24	0.30	0.95	32 ± 6	31 ± 2	32 ± 1	0.69 ± 0.07			
44	0.80	2.5	36 ± 6	71 ± 2	74 ± 1	1.1 ± 0.1			
ULP									
0.82	0.072	0.22	145 ± 3	8.4 ± 0.3	25 ± 0.5	3.1 ± 0.06			
1.8	0.093	0.29	167 ± 3	9.0 ± 0.2	37 ± 0.6	4.7 ± 0.04			
2.5	0.11	0.35	168 ± 7	9.8 ± 0.6	42 ± 0.6	5.3 ± 0.1			
6.4	0.26	0.79	180 ± 10	21 ± 1	87 ± 1	11 ± 0.1			
13	0.69	2.1	160 ± 10	52 ± 2	130 ± 2	15 ± 0.7			
DP									
1.4	0.076	0.24	250 ± 2	4.9 ± 0.1	36 ± 0.9	5.2 ± 0.07			
2.8	0.095	0.30	230 ± 30	6 ± 2	56 ± 2	8.9 ± 1			
3.9	0.11	0.35	262 ± 6	5.9 ± 0.2	77 ± 2	12 ± 0.2			
10	0.26	0.81	291 ± 9	20 ± 1	190 ± 4	25 ± 0.3			
19	0.60	1.9	299 ± 7	33 ± 1	460 ± 8	68 ± 2			

among the polymers. R_c is smaller than $l_{\rm Oh}$ for all USP solutions, but larger for ULP and DP solutions until $c > c^*$. The radius evolution of USP follows the VC scaling whereas the radii of ULP and DP scales as a power-law with an exponent of $n_e \sim 0.7 - 1$.

Extensional responses across PAM solutions differ significantly by polymer size, indicating that c^* is not a good scaling parameter to understand the molecular weight contributions. Polymer size strongly affects both the practical processing timescale t_f and the characteristic timescale of elasticity λ_E probed from DoS measurement. Large polymers can increase the timescale significantly at a smaller mass concentration, and both t_f and λ_E from DP solutions appear to be dominated by the larger polymers in the distributions. Overall, t_f is dominated by the EC regime, suggesting that polymer elasticity has stronger contributions and further analysis of λ_E may elucidate the physical picture of the behavior.

We apply the framework used in Ref. 24 to understand the role of polymer size by calculating macromolecular parameters as criteria for coil-stretch hysteresis. To determine whether our

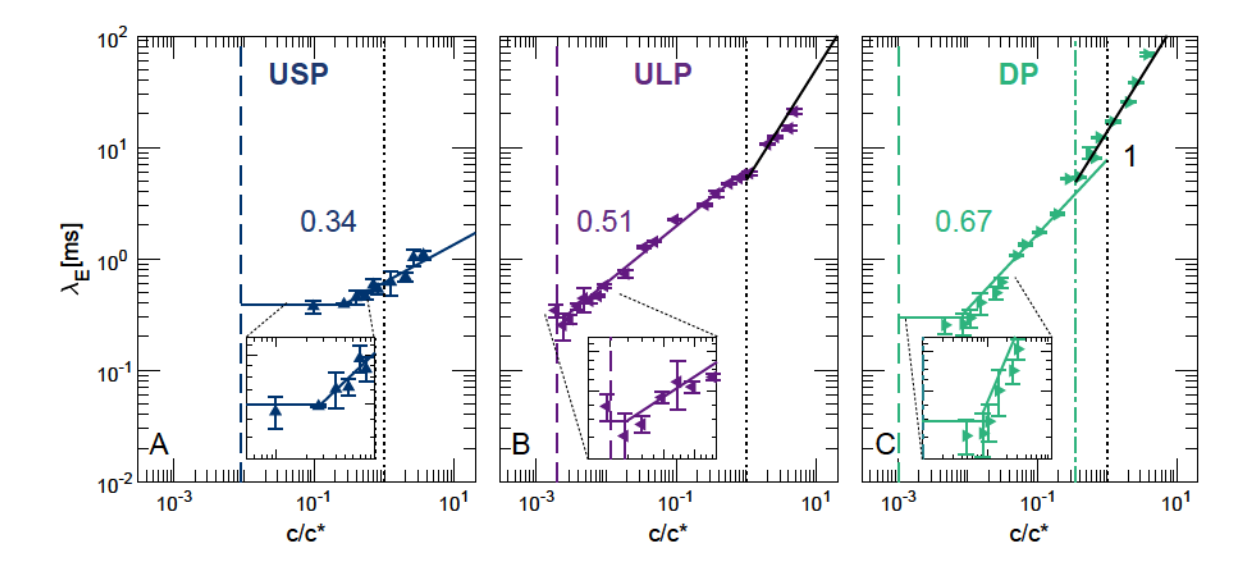


Figure 5: Extensional relaxation time $\lambda_{\rm E}$ for polyacrylamide solutions as a function of normalized concentration c/c^* . The dashed vertical lines indicate the predicted minimum concentration $c_{\rm min}$ needed to observe an elastocapillary response for each polymer. The black dotted vertical lines indicate the transition from dilute to semidilute regime. For DP solutions, the vertical dashed dotted line indicates the overlap concentration c^* derived from Mark-Houwink equation and M_w . Power-law exponents extracted from the fitting are 0.34 ± 0.06 for USP, 0.51 ± 0.02 for ULP, and 0.67 ± 0.07 for DP. Error bars are determined from the standard deviation of multiple replicates. Inset: Transition to concentration-independent regime of λ_E at low concentration limit.

PAM solutions exhibit coil-stretch hysteresis, we compare the ratio of the drag coefficient of stretched $\zeta_s = (2\pi\eta_s L_c)/\ln(L_c/d)$ and coiled $\zeta_c = (3/8)(6\pi^3)^{1/2}\eta_s R_{\rm us}$ chains,³ which are a function of the different polymer length scales (Fig.1D-F), to the criterion $\zeta_s/\zeta_c > 4.5$.²⁰

Here, we estimate contour length $L_{c,w} = \sin(\theta/2)N_w l_0$ from the degree of polymerization $N_w = M_w/M_0$. We consider both linear $\theta = 180^\circ$ and all-trans $\theta = 109.5^\circ$ configurations. The Kuhn segment diameter d is calculated from the packing length $p = (\pi/4)d_k^2/b_k \approx d^2/b_k$ and actual diameter $d_k = 4M_0/\sin(\theta/2)j\pi lN_{\rm av}\rho$, where j is the number of backbone bonds in the monomer, l is the bond length, $N_{\rm av}$ is Avogadro's number, and ρ is the polymer density. The polymer length scales, the radius of gyration 62 $R_{\rm g} = M_w/(4/3)\pi N_{av}c^*$ with $c^* = 1/[\eta]$ and the unstretched polymer length 3 $R_{\rm us} = R_g\sqrt{6}$, are determined from shear rheology under near-quiescent conditions. For DP, we use the value of $[\eta]$ estimated from

Table 2: Macromolecular parameters of polyacrylamide characterized from supplier information, intrinsic viscosity measurements, and estimation from molecular properties. The range of values arises from two bond angles (linear $\theta = 180^{\circ}$ and all-trans $\theta = 109.5^{\circ}$). Basic shared parameters are $M_0 = 71$ g mol⁻¹, $b_K = 1.1 - 1.3$ nm, and d = 0.6 nm.

Parameters		USP	ULP	DP
$[\eta] \; (\text{mL} \cdot \text{mg}^{-1})$	intrinsic viscosity	0.082	0.31	$0.54^{\mathrm{a}}, 0.20^{\mathrm{b}}$
$\lambda_{ m z} \; ({ m ms})$	Zimm relaxation time	0.19	3.8	4.8
$c^* \; (\text{mg} \cdot \text{mL}^{-1})$	overlap concentration	12	3.2	$5.1^{a}, 1.8^{b}$
$R_{\rm g}$ (nm)	radius of gyration	19	50	$36^{\rm a},75^{\rm b}$
R_{us} (nm)	unstretched polymer length	47	122	184
$N_{ m w}$	degree of polymerization	2732	14085	27746
$L_{\rm c}~({ m nm})$	contour length	687 - 842	3543 - 4338	6979 - 8546
$N_{\mathbf{k}}$	number of Kuhn segments	643 - 787	3315 - 4059	6530 - 7996
$L_{ m E}^2$	finite extensibility parameter	218 - 327	837 - 1255	1443 - 2164
$\zeta_{\rm s}/\zeta_{\rm c}$	drag coefficient ratio	2.5 - 3.0	4.0 - 4.8	4.9 - 5.9
$c_{\min}/c^*(\times 10^3)$	minimum concentration	8.6 - 13	2.2 - 3.4	1.3 - 2.0
$c_{ m s}/c^*(imes 10^2)$	overlap stretched concentration	20 - 30	14 - 21	12 - 18

^a Experimental measurement

 $M_{\rm w}$ to calculate the relevant parameters. We calculate the flexibility, represented by the number of Kuhn segments 3,24 $N_{\rm k} = L_{c,w}/b_k$, extensibility 6,24 $L_{\rm E}^2 = (L_{c,w}/R_{\rm us})^2$, and segmental dissymmetry 24 $S_{\rm d} = (b_k/d)^2$. Finally, we predict the delineation of concentrations using $c_{\rm min}/c^* = 3/2L_E^2 U_{\eta\tau}$, 35 and $c_s^*/c^* = (4/3)\pi R_g^3/dL_{c,w}^2$. All relevant parameters are tabulated in Table 2.

For low c/c^* , λ_E is independent of concentration (Fig. 5), as expected for $c_{\min} < c < c_s^*$. We determine the concentration-independent regime as the regime in which the relaxation time is equal within the standard deviation. The prediction of the transition from the polymer macromolecular parameters $c_s^*/c^* \approx N_k(b_k/d)/L_E^3$, where N_k is the number of Kuhn segments, d is the hydrodynamic bead diameter, and L_E^2 is the extensibility, ²⁴ is within an order of magnitude of our experimental results. The consistency between the experimentally-measured and theoretically-predicted values of c_s^* supports the use of macromolecular parameters to delineate the concentration regimes.

Using the linear configuration, we estimate for USP $\zeta_s/\zeta_c < 4.5$ and for ULP and DP $\zeta_s/\zeta_c > 4.5$, indicating that coil-stretch hysteresis occurs in ULP and DP solutions but not

^b Estimated from $[\eta] = kM_v^a$

in USP solutions. ^{20,24} The experimentally measured scaling exponents of $\lambda_{\rm E}$ with concentration are consistent with the calculated ζ_s/ζ_c : $m_{\rm USP}=0.34\pm0.06$, close to 0.31 predicted for hydrodynamic interactions, and $m_{\rm ULP}=0.51\pm0.02$ and $m_{\rm DP}=0.67\pm0.07$, close to the geometric mean of the two limiting exponents and indicative of EV screening. The increase in drag coefficient ratio between ULP and DP is due to M_w of DP, which is almost twice that of ULP, and may also contribute to the degree of partial EV screening, as $m_{\rm DP}>m_{\rm ULP}$.

At greater concentrations, the scaling exponent transitions to unity for ULP and DP solutions. This transition occurs at c^* for ULP solutions, as expected for full screening of the EV interactions. For DP solutions, however, the transition to linear scaling occurs at $c/c^* \sim 0.28$. This value is close to the overlap concentration of DP derived from Mark-Houwink parameters from USP and ULP solutions using the M_w of DP, $c/c^* \sim 0.35$. This result suggests that the transition to semidilute regime under extensional flow may be better described by overlap concentration c^* that is representative of M_w instead of M_v obtained from shear rheology.

An earlier study of the capillary breakup of PAM with $M_w = 5-6$ MDa in glycerol-water mixtures³⁹ found the power-law exponent exhibited a stronger concentration dependence $(m=0.82\pm0.04)$ over a range of concentrations spanning c^* . This value is comparable to the exponent obtained by fitting our DP data from $c_s^* < c < c^*$ $(m_{\text{DP,span}} = 0.85\pm0.09)$. Thus, whereas the higher exponent in their study may be due to the increase in EV screening as some data points were in the $c > c^*$ regime, our results suggest that this stronger concentration dependence may arise from a shift of effective c^* due to high dispersity. The importance of high molecular weight polymers in the extensional rheology of disperse polymer solutions is consistent with earlier observations of the spinnability of disperse polymer solutions. 41,42

From the scaling relationship, we also examine the monomer relaxation time $\lambda_0 \approx \eta_s b^3/kT$ which can be substituted into eqn. 1 as a way to quantitatively predict the concentration-

dependence of the relaxation time across molecular weight. ³⁰ When the segment length is approximated as $b_k \approx 1.1$ nm, the predicted λ_0 is 18 ns. We find that when λ_0 is extracted from the slope of λ_E scaling, we obtain 0.25, 0.33 and 0.16 ns from USP, ULP, and DP respectively, differing from the value predicted from the segment length. The λ_0 values extracted from λ_E , however, could predict Zimm relaxation time $\lambda_z \approx \lambda_0 N^{3\nu}$ within an order of magnitude, as also found in PEO in water system. ³⁰ The predicted λ_z is close to the value corresponding to the weight-averaged estimated $[\eta]$, which supports our conclusion that weight-averaged parameter better predicts the extensional response of the polymer solutions.

Conclusion

Our study connects the macromolecular parameters to the concentration-dependent extensional response of polyacrylamide (PAM) solutions under extensional flow and intriguingly suggests that we can vary polymer size and dispersity as an option to tailor the material response. The polymer size qualitatively controls the pinch-off dynamics, where larger polymers (ULP and DP) introduce a distinct transition to elastocapillary (EC) regime that is characterized by the discrete overshoot in strain rate. These differences are not observed in the shear rheology characterization when compared at similar normalized concentration c/c^* in the dilute regime $c/c^* < 1$. As polymer concentration increases, the concentration-dependent response in EC regime exhibits a power-law scaling that depends on polymer size. The scaling exponents characterizing the concentration dependence of $\lambda_{\rm E}$ increase with ς_s/ς_c , (i.e. $m_{\rm USP} < m_{\rm ULP} < m_{\rm DP}$), consistent with previous studies. ^{24,30}

The full screening of EV interactions also depends on the overlap concentration c^* determined from M_w , leading to a transition to linear scaling at lower c in highly disperse solutions. This result indicates that the larger polymers in a polydisperse mixture contribute more significantly to the solution dynamics.

Future studies in more complicated systems such as polyelectrolytes are expected to provide additional insight into factors controlling concentration-dependent material response for applications in polymer processing and advanced manufacturing.

Acknowledgement

The authors thank Megan Robertson for access to the DHR-2 Rheometer, Alamgir Karim for access to the KronTech high-speed camera, Gerald Blosser for machining of DoS setup, and Christopher Macosko for constructive discussions. JCC acknowledges funding from the National Science Foundation (CBET-1803728) and the Welch Foundation (E-1869).

Supporting Information Available

Protocols for shear rheology and DoS; additional calculation of the macromolecular parameters of PAM, summarized in Table 2; gel permeation chromatography traces of the polymers; captions for Movies S1 – S3.

References

- (1) de Gennes, P.-G. Scaling Concepts in Polymer Physics; Cornell University Press: Ithaca, 1979.
- (2) Doi, M.; Edwards, S. F.; Edwards, S. F. The Theory of Polymer Dynamics; Oxford University Press: New York, 1986.
- (3) Larson, R. G. The Structure and Rheology of Complex Fluids; Oxford University Press: New York, 1999.

- (4) Macosko, C. W. Rheology: Principles, Measurements, and Applications; VCH: New York, 1994.
- (5) Rubinstein, M.; Colby, R. H. Polymer Physics; Oxford University Press: New York, 2003.
- (6) Larson, R. G. The rheology of dilute solutions of flexible polymers: Progress and problems. J. Rheol. 2005, 49, 1–70.
- (7) Mishra, R.; Militky, J.; Venkataraman, M. In Nanotechnology in Textiles; Mishra, R., Militky, J., Eds.; The Textile Institute Book Series; Woodhead Publishing: Duxford, 2019; pp 35–161.
- (8) Jiang, Z.; Diggle, B.; Tan, M. L.; Viktorova, J.; Bennett, C. W.; Connal, L. A. Extrusion 3D Printing of Polymeric Materials with Advanced Properties. Adv. Sci. 2020, 7, 2001379.
- (9) Prakash, J. R. Universal dynamics of dilute and semidilute solutions of flexible linear polymers. Curr. Opin. Colloid Interface Sci. 2019, 43, 63–79.
- (10) Matsumiya, Y.; Watanabe, H. Non-universal features in uniaxially extensional rheology of linear polymer melts and concentrated solutions: A review. Prog. Polym. Sci. 2021, 112, 101325.
- (11) Petrie, C. J. One hundred years of extensional flow. J. Nonnewton. Fluid Mech. 2006, 137, 1–14.
- (12) Dinic, J.; Martínez Narváez, C. D. V.; Sharma, V. Macromolecular Engineering; John Wiley & Sons, Ltd: Chichester, 2022; pp 1–36.
- (13) McKinley, G. H. Visco-elasto-capillary thinning and break-up of complex fluids. Rheol. Rev. 2005, 1–48.

- (14) Schroeder, C. M. Single polymer dynamics for molecular rheology. J. Rheol. 2018, 62, 371–403.
- (15) de Gennes, P.-G. Coil-stretch transition of dilute flexible polymers under ultrahigh velocity gradients. J. Chem. Phys. 1974, 60, 5030–5042.
- (16) Tanner, R. I. Stresses in Dilute Solutions of Bead-Nonlinear-Spring Macromolecules. III. Friction Coefficient Varying with Dumbbell Extension. Trans. Soc. of Rheol. 1975, 19, 557–582.
- (17) Hinch, E. J. Mechanical models of dilute polymer solutions in strong flows. The Physics of Fluids 1977, 20, S22–S30.
- (18) Schroeder, C. M.; Babcock, H. P.; Shaqfeh, E. S.; Chu, S. Observation of polymer conformation hysteresis in extensional flow. Science 2003, 301, 1515–1519.
- (19) Schroeder, C. M.; Shaqfeh, E. S.; Chu, S. Effect of hydrodynamic interactions on DNA dynamics in extensional flow: Simulation and single molecule experiment. *Macro-molecules* 2004, 37, 9242–9256.
- (20) Hsieh, C.-C.; Larson, R. G. Prediction of coil-stretch hysteresis for dilute polystyrene molecules in extensional flow. J. Rheol. 2005, 49, 1081–1089.
- (21) Hsieh, C.-C.; Li, L.; Larson, R. G. Modeling hydrodynamic interaction in Brownian dynamics: simulations of extensional flows of dilute solutions of DNA and polystyrene. J. Nonnewton. Fluid Mech. 2003, 113, 147–191.
- (22) Hsieh, C.-C.; Larson, R. G. Modeling hydrodynamic interaction in Brownian dynamics: Simulations of extensional and shear flows of dilute solutions of high molecular weight polystyrene. J. Rheol. 2004, 48, 995–1021.
- (23) Prabhakar, R. Enhancement of coil-stretch hysteresis by self-concentration in polymer

- solutions. arXiv (Soft Condensed Matter), January 31, 2013; 1209.0163, Ver.2. https://arxiv.org/abs/1209.0163 (accessed April 4, 2023).
- (24) Dinic, J.; Sharma, V. Flexibility, Extensibility, and Ratio of Kuhn Length to Packing Length Govern the Pinching Dynamics, Coil-Stretch Transition, and Rheology of Polymer Solutions. *Macromolecules* 2020, 53, 4821–4835.
- (25) Dunlap, P.; Leal, L. Dilute polystyrene solutions in extensional flows: Birefringence and flow modification. J. Nonnewton. Fluid Mech. 1987, 23, 5–48.
- (26) Pincus, P. Excluded volume effects and stretched polymer chains. *Macromolecules* 1976, 9, 386–388.
- (27) Prabhakar, R.; Gadkari, S.; Gopesh, T.; Shaw, M. Influence of stretching induced self-concentration and self-dilution on coil-stretch hysteresis and capillary thinning of unentangled polymer solutions. J. Rheol. 2016, 60, 345–366.
- (28) Prabhakar, R.; Sasmal, C.; Nguyen, D. A.; Sridhar, T.; Prakash, J. R. Effect of stretching-induced changes in hydrodynamic screening on coil-stretch hysteresis of unentangled polymer solutions. *Phys. Rev. Fluid* 2017, 2, 011301.
- (29) Harrison, G. M.; Remmelgas, J.; Leal, L. G. The dynamics of ultradilute polymer solutions in transient flow: Comparison of dumbbell-based theory and experiment. J. Rheol. 1998, 42, 1039–1058.
- (30) Dinic, J.; Biagioli, M.; Sharma, V. Pinch-off dynamics and extensional relaxation times of intrinsically semi-dilute polymer solutions characterized by dripping-onto-substrate rheometry. J. Polym. Sci. B Polym. Phys. 2017, 55, 1692–1704.
- (31) Dinic, J.; Zhang, Y.; Jimenez, L. N.; Sharma, V. Extensional relaxation times of dilute, aqueous polymer solutions. ACS Macro Lett. 2015, 4, 804–808.

- (32) Dinic, J.; Jimenez, L. N.; Sharma, V. Pinch-off dynamics and dripping-onto-substrate (DoS) rheometry of complex fluids. Lab Chip 2017, 17, 460–473.
- (33) Dinic, J.; Sharma, V. Macromolecular relaxation, strain, and extensibility determine elastocapillary thinning and extensional viscosity of polymer solutions. *Proc. Natl.* Acad. Sci. U.S.A. 2019, 116, 8766–8774.
- (34) Bousfield, D.; Keunings, R.; Marrucci, G.; Denn, M. Nonlinear analysis of the surface tension driven breakup of viscoelastic filaments. J. Nonnewton. Fluid Mech. 1986, 21, 79–97.
- (35) Clasen, C.; Plog, J.; Kulicke, W.-M.; Owens, M.; Macosko, C.; Scriven, L.; Verani, M.; McKinley, G. H. How dilute are dilute solutions in extensional flows? J. Rheol. 2006, 50, 849–881.
- (36) Muthukumar, M.; Freed, K. F. Theory of concentration dependence of polymer relaxation times in dilute solutions. *Macromolecules* 1978, 11, 843–852.
- (37) Daoud, M.; Cotton, J.; Farnoux, B.; Jannink, G.; Sarma, G.; Benoit, H.; Duplessix, C.; Picot, C.; De Gennes, P. Solutions of flexible polymers. Neutron experiments and interpretation. *Macromolecules* 1975, 8, 804–818.
- (38) Tirtaatmadja, V.; McKinley, G. H.; Cooper-White, J. J. Drop formation and breakup of low viscosity elastic fluids: Effects of molecular weight and concentration. *Phys. Fluids* 2006, 18, 043101.
- (39) Zell, A.; Gier, S.; Rafaï, S.; Wagner, C. Is there a relationship between the elongational viscosity and the first normal stress difference in polymer solutions? J. Nonnewton. Fluid Mech. 2010, 165, 1265–1274.
- (40) Bazilevskii, A.; Entov, V.; Rozhkov, A. Breakup of an Oldroyd liquid bridge as a method

- for testing the rheological properties of polymer solutions. *Vysokomol. Soedin., Ser. A Ser. B1023-3091* **2001**, 43, 716–726.
- (41) Merchiers, J.; Reddy, N. K.; Sharma, V. Extensibility-Enriched Spinnability and Enhanced Sorption and Strength of Centrifugally Spun Polystyrene Fiber Mats. *Macro-molecules* 2022, 55, 942–955.
- (42) Palangetic, L.; Reddy, N. K.; Srinivasan, S.; Cohen, R. E.; McKinley, G. H.; Clasen, C. Dispersity and spinnability: Why highly polydisperse polymer solutions are desirable for electrospinning. *Polymer* 2014, 55, 4920–4931.
- (43) Malkin, A. Y.; Semakov, A. V.; Skvortsov, I. Y.; Zatonskikh, P.; Kulichikhin, V. G.; Subbotin, A. V.; Semenov, A. N. Spinnability of Dilute Polymer Solutions. *Macro-molecules* 2017, 50, 8231–8244.
- (44) Merchiers, J.; Slykas, C. L.; Martínez Narváez, C. D. V.; Buntinx, M.; Deferme, W.; Peeters, R.; Reddy, N. K.; Sharma, V. Fiber Engineering Trifecta of Spinnability, Morphology, and Properties: Centrifugally Spun versus Electrospun Fibers. ACS Appl. Polym. Mater. 2022, 4, 2022–2035.
- (45) Merchiers, J.; Martínez Narváez, C. D. V.; Slykas, C.; Reddy, N. K.; Sharma, V. Evaporation and Rheology Chart the Processability Map for Centrifugal Force Spinning. Macromolecules 2021, 54, 11061–11073.
- (46) Sitaramaiah, G.; Smith, C. L. Turbulent Drag Reduction by Polyacrylamide and Other Polymers. SPE J. 1969, 9, 183–188.
- (47) Mungan, N.; Smith, F.; Thompson, J. Some Aspects of Polymer Floods. J. Pet. Technol. 1966, 18, 1143–1150.
- (48) Lu, P.; Hsieh, Y.-L. Organic compatible polyacrylamide hydrogel fibers. *Polymer* 2009, 50, 3670–3679.

- (49) Desai, K.; Kit, K. Effect of spinning temperature and blend ratios on electrospun chitosan/poly (acrylamide) blends fibers. *Polymer* **2008**, *49*, 4046–4050.
- (50) Odell, J.; Keller, A. Flow-induced chain fracture of isolated linear macromolecules in solution. J. Polym. Sci. B Polym. Phys. 1986, 24, 1889–1916.
- (51) Odell, J.; Keller, A.; Rabin, Y. Flow-induced scission of isolated macromolecules. J. Chem. Phys. 1988, 88, 4022–4028.
- (52) Odell, J. A.; Muller, A. J.; Narh, K. A.; Keller, A. Degradation of polymer solutions in extensional flows. *Macromolecules* **1990**, *23*, 3092–3103.
- (53) Park, N.; Umanzor, E. J.; Conrad, J. C. Aqueous Colloid+ Polymer Depletion System for Confocal Microscopy and Rheology. Front. Phys. 2018, 6, 42.
- (54) Kulicke, W.-M.; Kniewske, R.; Klein, J. Preparation, characterization, solution properties and rheological behaviour of polyacrylamide. *Prog. Polym. Sci.* **1982**, *8*, 373–468.
- (55) Papageorgiou, D. T. On the breakup of viscous liquid threads. Phys. Fluids 1995, 7, 1529–1544.
- (56) Martínez Narváez, C. D.; Dinic, J.; Lu, X.; Wang, C.; Rock, R.; Sun, H.; Sharma, V. Rheology and pinching dynamics of associative polysaccharide solutions. *Macro-molecules* 2021, 54, 6372–6388.
- (57) McKinley, G. H.; Tripathi, A. How to extract the Newtonian viscosity from capillary breakup measurements in a filament rheometer. J. Rheol. 2000, 44, 653–670.
- (58) Fardin, M. A.; Hautefeuille, M.; Sharma, V. Spreading, pinching, and coalescence: the Ohnesorge units. *Soft Matter* **2022**, *18*, 3291–3303.
- (59) Chen, Y.-J.; Steen, P. Dynamics of inviscid capillary breakup: collapse and pinchoff of a film bridge. J. Fluid Mech. 1997, 341, 245–267.

- (60) Day, R. F.; Hinch, E. J.; Lister, J. R. Self-similar capillary pinchoff of an inviscid fluid. Phys. Rev. Lett. 1998, 80, 704–707.
- (61) Entov, V.; Hinch, E. Effect of a spectrum of relaxation times on the capillary thinning of a filament of elastic liquid. J. Nonnewton. Fluid Mech. 1997, 72, 31–53.
- (62) Wolff, C. Molecular weight dependence of the relative viscosity of solutions of polymers at the critical concentration. Eur. Polym. J. 1977, 13, 739–741.

TOC Graphic

